The Temperature of the Cosmic Microwave Background at 3 mm

Jeffrey Schuster[1], Todd C. Gaier[2], Timothy Koch[3], Michael D. Seiffert[2], and Philip M. Lubin[2]

Received _____; accepted _____

As submitted
7/11/95

[1]Current mailing address:

[2]Physics Department, University of California Santa Barbara, Santa Barbara, CA 93...

[3]Jet Propulsion Laboratory, California Institute of Technology, 4800 Oak Grove Dr...
Pasadena, CA 91109

ABSTRACT

We report here on a narrow band measurement of the temperature of the cosmic background radiation. The measurement employed two Schottky diode based heterodyne radiometers, one at a fixed center frequency of 90 GHz, the other tunable from 85-100 GHz. This configuration gave powerful checks of possible systematic effects. The instrument was flown on a balloon platform to reduce the level of atmospheric emission to $\simeq$ 1 mK. The two radiometers made measurements of T_{CMB} with a weighted average of $2.717 \pm .017$ K, comparable to the most sensitive measurements made to date.

Subject headings: cosmic microwave background — cosmology:observations — early universe

1. INTRODUCTION

An expanding universe immediately implies an earlier, denser state, and taken to its extreme, an infinitely hot, dense universe. This simple prediction is the hot big bang, the basis of the standard model of cosmology. In the 1940's it was realized that the early, hot universe should have left a radiation background that cooled as the universe expanded, the Cosmic Microwave Background (CMB). Early calculations that required that the number density of nucleons be sufficient to make elements heavier than hydrogen when the universe was at 10^9 K predicted the existence of the CMB with a temperature of $\simeq 5$ K at the present time (Gamow 1946; Alpher 1950). In the early 1960's, a group of physicists at Princeton university, led by R. H. Dicke and P. J. E. Peebles began an experimental program to measure the temperature of the CMB. In 1965, Arno Penzias and Robert Wilson made the first measurement of this temperature, $T_{CMB} = 3.5 \pm 1$ K (Penzias & Wilson 1965). This value is within 1σ of modern measurements.

The CMB, being composed of photons that have not interacted with the universe since it was less than 1 million years old, is currently the best probe of the very early universe. Any energy injection after a redshift of 10^7 will not be entirely thermalized, and thus will give rise to distortions in an otherwise Planck spectrum. For energy injection in the range $10^7 > z > 10^4$, the CMB can come to kinetic but not thermal equilibrium, because all processes that change the number of photons are slower than the expansion rate of the universe. At low frequencies, Bremsstrahlung radiation can bring about thermal equilibrium. Thus the spectrum can be characterized by a chemical potential, μ, that is damped at low frequencies (Sunyaev & Zel'dovich 1970)

$$\mu(x) = \mu_0 \exp\left[-2x_1/x\right] \quad (1)$$

where x_1 is the frequency of transition from a Planck to a Bose-Einstein spectrum and μ_0 is

roughly the fractional amount of energy injected into the CMB. x_1 is often lower than the frequencies of interest. The photon occupation number, $n(x)$, is then given by the standard expression:

$$n\left(x\right) = \frac{1}{\exp\left[x + \mu\left(x\right)\right] - 1} \tag{2}$$

After $z = 10^4$, Compton scattering lifts photons from the Raleigh-Jeans portion of the spectrum to the Wein tail, a process characterized by the "Compton y parameter" (Sunyaev & Zel'dovich 1969):

$$y = \int \frac{k\left(T_e - T_{CMB}\right)}{m_e c^2} \sigma_T N_e dl \tag{3}$$

where the integral is along the line of sight. The antenna temperature distortion in the Raleigh Jeans portion of the spectrum is $\simeq -2y$. The effects of other processes, involving cosmic strings (Ponce & Vishniac 1988; Sanchez & Signore 1990), dust (Negroponte et al. 1981), anisotropic expansion (Rees 1968), and other causes have also been calculated.

Since the initial work of Penzias and Wilson, many measurements of T_{CMB} of steadily improving precision have been made. Longward of 3 mm, a number of ground based measurements have been made using coherent detectors. Combining data taken in 1988 and 1989 from the South Pole and White Mountain, Bensadoun et al. (1993) report $T_{CMB} = 2.26 \pm 0.19$ K. At the wavelength of the measurement reported here, Bersanelli et al. (1989) measure $T_{CMB} = 2.60 \pm 0.09$ K. At 1.2 cm, the group at Princeton reported a very sensitive balloon borne measurement of $T_{CMB} = 2.783 \pm 0.025$ (Johnson & Wilkinson 1987).

An entirely different way of measuring T_{CMB} uses the 3874 line strengths of interstellar CN to measure the excitation temperature of the $J = 0 - 1$ rotational transition at 2.64 mm (Meyer & Jura, 1985). This technique has given a measured temperature of $T_{CMB} = 2.796 + 0.014, -0.039$ K (Crane et al. 1989). Recently, a similar measurement using orthoformaldehyde in the direction of the giant HII region W51A yielded $T_{CMB} = 3.2 \pm 0.9$

K (Kogut et al. 1990).

The launch of the Cosmic Background Explorer on 1989 November 18 ushered in a new era of CMB measurements. The Far Infrared Absolute Spectrometer (FIRAS), with its bolometric Fourier transform spectrometer, measured a temperature of $T_{CMB} = 2.726 \pm 0.010$ K (Mather et al. 1993), and placed limits on distortions of the spectrum of $y < 2.5 \times 10^{-5}$, and $\mu < 3.3 \times 10^{-4}$ (Wright et al. 1993). A similar rocket based instrument, COBRA, gave the result $T_{CMB} = 2.736 \pm 0.017$ K (Gush et al. 1990).

Recently, more emphasis has been placed on lower frequency measurements. This is due in part to the excellent FIRAS and COBRA measurements, and in part because of the large μ type distortions expected there. Although these experiments have greater difficulties with optics and contamination from galactic synchrotron emission, progress has been made. At 600 MHz, the value $T_{CMB} = 3 \pm 1.2$ K has been measured (Sironi et al. 1990).

2. THE INSTRUMENT

2.1. THE OPTICS

In any absolute measurement of the temperature of the CMB, care must be taken to avoid systematic errors. At some level, radiation from warm objects surrounding the experiment will enter the radiometer, and this radiation is often indistinguishable from the CMB. In order to minimize possible offsets from warm optics, our system was coupled quasi-optically to the CMB, with each radiometer using a single cold (< 10 K) off axis ellipsoidal mirror with foci at 6.858 and 50.8 cm (see Figure 1). These mirrors were fed by 20° semi-flare angle scalar feed horns with 2.5 cm apertures. This combination led to a 10 beam (FWHM) on the sky. The foci of the ellipsoidal mirrors were defined by two criteria In order to minimize any pick-up of thermal emission from the warm exit aperture of the

instrument, the apertures of the feed horns were imaged onto the mouth of the cryostat, stopping the beam at this point. Because there is no radiation received by the instrument from outside of the walls of the feed horn, there should be none received from outside of the image of the horn in the image plane, where the warm surfaces are. Additionally, the beam waist (narrowest part of the beam) was placed at the entrance to the calibrator. This minimized any pickup from the light pipe that directed the beam into the calibrator. It also allowed the entrance to the calibrator to be as small as possible, minimizing possible heating of the emitting surface.

The beam was chopped between the sky and the calibrator every 26 seconds using a flat gold plated polished aluminum mirror. In addition to continuously calibrating the experiment, this chop acted as a Dicke switch to reduce $1/f$ type noise. Because the chop was relatively slow, there was excess low frequency noise left in the final data. The symmetry inherent in this chopping mirror allowed for a second system with identical optics to placed on the opposite side, receiving radiation from the sky when the first system is being calibrated. This second system, operating at a different frequency, allowed for powerful tests of many potential systematic errors. Although it was possible to operate both systems simultaneously, during the flight only one local oscillator was turned on at any given time. This was done to eliminate any possible cross talk between the two systems.

The cold calibrator was a blackbody emitter, using Eccosorb CR-110 as the absorbing medium. To increase emissivity and reduce the size of any potential standing wave, the front surface was conical and coated with a $\lambda/4$ thick Teflon anti-reflection coating. This gave a measured return loss of -61 dB. Temperature gradients were minimized by using 10 ppm impurity copper throughout, and the temperature gradient across the calibrator was measure in the laboratory to be less than 5 mK. Any potential standing wave was measured and removed (see §4) by positioning the calibrator in precise $\lambda/20$ steps, giving a round

trip path difference of $\lambda/10$. The temperature could be set anywhere from 2 K to 5 K, and controlled at a precision of better than 10 mK.

The temperature was measured and controlled using germanium resistance thermometers (GRTs). A single read circuit was multiplexed to 3 GRTs. It also measured the resistance of 3 high stability reference resistors mounted on a temperature controlled plate. These reference resistors were used for a real time calibration. The entire apparatus is described in detail in another publication (Schuster & Lubin, 1994).

2.2. THE RF SYSTEM

The first of the two systems mentioned in the previous section (hereafter system "B") operated at 90 GHz, with two side bands of width 550 MHz each centered 1275 MHz above and below the local oscillator frequency. A ring coupler resonantly coupled the local oscillator power onto the Schottky diode mixer. This system often operated during laboratory testing with a system noise temperature below 200 K. However, a slight local oscillator frequency shift during the launch of the flight resulted in a noise temperature of 650 K. However, this proved to be sensitive enough for this measurement. For the other system (system "A"), the system temperature was compromised to allow for a radiometer that could be tuned from 85-110 GHz during the flight. This tuning was accomplished with a closed loop servo that drove two gear motors that positioned the tuning and back-short micrometers on the local oscillator to a precision of 0.0002". The frequency could be set with an rms error of 200 MHz, and most of this error came from a few resonant points on the tuning curve. System "A" had a system temperature of 630 K, and side bands of width 590 MHz, centered 1375 MHz above and below the local oscillator frequency.

2.3. THE IF AND DATA ACQUISITION SYSTEMS

Figure 2 shows schematically the RF and IF systems. The intermediate frequency signals were amplified by cold HEMT amplifiers, and then brought out of the cryostat and further amplified. They were then passed through tubular filters to define the bandpasses and -60 dB notch filters that removed the telemetry transmitter signal. System "B" required an isolator between the warm and cold amplifiers to eliminate a standing wave. Finally, the signals were rectified by detector diodes, integrated for 1 second using an ideal integrator circuit, and read into the computer. Once in the computer, the data were written to an on board hard disk, giving a data set free of transmission errors. The data were also transmitted to the ground for real time analysis.

2.4. HOUSEKEEPING AND CONTROL SYSTEMS

The on board computer used an 80186 microprocessor. In addition to scientific data, it also acquired housekeeping data, such as temperatures, pressures, and gondola pointing information. The computer was also used to control many electro-mechanical servo systems, and precisely control the temperature of the cold calibrator. The servo systems that turned on the motor that rotated the entire balloon gondola and opened the aperture cover once the desired altitude was achieved were simple systems utilizing relays. The entire gondola was rotated using a Miller swivel that was driven by a planetary gear-head motor (see Figure 3). The aperture cover was opened (and closed at the end of the flight) by another D.C. gear motor that drove a worm gear. This cover also was used as a large signal calibrator. Inside the cover was a black body emitter. It was fabricated using a polystyrene mold that formed the front surface of the absorber into grooves to reduce reflections. This polystyrene was left in place as insulation to reduce potential temperature gradients. Calibrated silicon diode temperature sensors were used to measure the temperature of this warm calibrator

as well as the cold plate temperature.

The elevation angle of the system was controlled by a closed loop analog servo system which utilized an H-switch to drive a D.C. linear actuator. Because of our large beam (10° FWHM) a simple potentiometer was adequate for feedback. This control system allowed the cryostat to be positioned in a compact, upright position for launch and landing, and then tilted as far as 45° from zenith to avoid the balloon and gondola super-structure. The cold calibrator had to be precisely positioned during flight in steps of 0.165 mm, to check for a potential standing wave (see §2.1). This was achieved using a closed loop control circuit and a planetary gear-head motor which was modified to operate at a temperature of 4 K. Additionally, the temperature of this calibrator had to be controlled at a precision of 10 mK. To do this, we implemented a software proportional-integral-derivative (PID) control using germanium resistance thermometers for feedback.

The chopper mirror was driven by a D.C. gear motor mounted at the aperture of the dewar. A miniature pitch chain moved the cold mirror. Positioning screws on the mirror stopped it in the up (CMB) or down (calibrator) positions. Stainless steel springs replaced a section of the chain to secure the mirror in place. These springs also allowed the motor to continue past the stopped position and hit limit switches, which turned off the drive current. These limit switches were also monitored by the computer to insure proper operation.

All of these systems could be controlled remotely from the ground through telemetry. Should our telemetry uplink have failed and a command was not received from the ground for a preset amount of time, the computer was programmed to take control and automatically make a series of measurements. This feature was not required during the flight. The data were telemetered to the ground through the National Scientific Balloon Facility's (NSBF's) Consolidated Instrument Package (CIP) transmitter.

3. THE FLIGHT

The data presented here were acquired during a flight that originated from Palestine, Texas, on 1991 May 25. The launch occurred at 1:57 UT, and the flight continued until 13:50 UT, at which time the liquid helium level fell to a level that was no longer capable of maintaining the temperature of the calibrator. The balloon had a volume of 0.33 million cubic meters (11.6 million cubic feet) and it initially carried our 636 kg payload to a maximum altitude of 37.2 km, and then stabilized at our desired altitude of 36 km. During the flight, the balloon traveled 590 km, slightly north of due west. After touching down and before the parachute was disconnected, the package was carried by the surface winds for approximately 100 m, severely damaging the payload. However, the computer survived, and the flight data were recovered from the hard disk.

Upon reaching the desired float altitude, the instrument aperture cover was successfully opened. With system "B" on and the local oscillator for system "A" off, data were acquired while the calibrator was stepped upward by 12 $\lambda/20$ steps, with the calibrator temperature set at 2.735 K. This we will call data set 1. Next, a long period of data was taken without moving the calibrator, as a check of the non-thermal offset of system "A." Subsequently, the gain of both systems was calibrated by changing the calibrator temperature to 5.735 K and then back to 2.735 K (see Figure 4). Then, with system "B" off and system "A" tuned to 98.8 GHz, another calibrator scan was performed (data set 2). This data set also constituted the baseline measurement for system "B". It was noted, however, that moving the calibrator caused a large exponentially decaying drift in the output of system "A", which we have attributed to heating the HEMT amplifier by the motor that positioned the calibrator. This effect limited the sensitivity of this data set to > 100 mK, and for this reason we will not discuss it further. At this point, we acquired a final science data set (data set 3) by allowing system "A" to equilibrate, moving the load by three or four steps

and again allowing system "A" to come to thermal equilibrium. Finally, we performed a zenith scan with both systems on to check for atmospheric contamination. During this scan, system "A" was tuned to 100.3 GHz so that the ozone line at 101.5 GHz was in the upper side band. At this point, the calibrator started to warm up, and so the aperture cover was closed, large signal calibrations were done at each frequency that was used during the flight, the dewar was moved to its "stow" position of 4°, and the payload was detached from the balloon and the gondola returned to earth.

4. DATA REDUCTION

As mentioned in the previous section, the small signal system gain was measured by ramping the temperature of the calibrator by 3 K. By doing a least squares fit of the calibrator temperature to the chopped offset, the gains were determined to be 35.6 mV/K for system "A" and 27.8 mV/K for system "B", when system "B" was at 98.8 GHz (see Figure 4). These calibrations approximately agree with the large signal calibrations and are considered more reliable because of the better coupling of the beam to the cold calibrator and because of the better knowledge of the cold calibrator's temperature. Small signal calibrations are also less sensitive to gain non-linearities. These calibrations are in thermodynamic temperature.

To analyze data sets 1 and 3, the raw data were stripped out of the data stream, along with such information as the chopper mirror and calibrator positions. Next, when the system was in the "down" position (beam coupled into the calibrator), the calibrator temperature times the system gain was subtracted from the output, insuring that the final result was the measured sky temperature. This also caused the measured RMS of the data to contain the variations in calibrator temperature (less than 10 mK) rather than trying account for those variations *a postiori* as a systematic error. Next, an RMS is calculated

at each load position, and this RMS is used to determine the final error bars. Because of the drifts discussed earlier, the data are cut on RMS and outliers are removed. However, over a broad range of values of these cuts, data set 3 varies by less than 10 mK. Data set 1 is almost independent of these cuts. Next, at each calibrator position, the data are simultaneously fit to linear and quadratic drifts and a mirror chop offset. Because of the relatively slow chop, these drifts are not insignificant. It is encouraging, however, that the results do not differ significantly from when no drifts were fit to the data. This is to be expected because the mirror chop offset, for long data sets, is almost orthogonal to a linear or quadratic drift. Finally, both components of a standing wave as a function of calibrator position and an overall offset were fit to the data. Data set 1 showed a significant standing wave (see Figure 5a). Because of the previously discussed shift of the local oscillator frequency for system "B", the ring coupler was no longer exactly resonant, and this caused some local oscillator power to leak out the front end of the system. We have ascribed the standing wave to this effect. Because of the excellent absorbtivity of our calibrator, no standing wave was observed in any measurement taken with system "A". Figure 5a shows data set 1 after binning by calibrator position, with the best fit standing wave. Figure 5b shows the residuals of the standing wave fit. Because of the presence of $1/f$-type noise in this data, it was decided to not divide the error bars by the square root of the number of calibrator positions, because $1/f$ noise need not integrate down as $\sqrt{n}$. All quoted values are given in thermodynamic temperature.

5. SYSTEMATIC ERRORS

During the design phase of this instrument, the philosophy was to examine all of the systematic errors that dominated the error budgets of previous measurements, and to what ever extent possible, reduce them below the level of 1 mK. To a large extent,

we were successful. Any difference between observing the calibrator and the sky causes an offset, giving an error in the measurement of T_{CMB}. By coupling the CMB into the system quasi-optically, using only cooled optics, we eliminated any significant emission from warm optics. A window at the dewar aperture would be emissive, and additionally could contribute to the standing wave, so it was eliminated. Any window on the calibrator could also cause an offset, and therefore we filled the light pipe that coupled the beam into the absorber with a blue polystyrene plug, which had a conical front surface to reduce reflections. To reduce the contributions of uncertainties in the overall instrument gain, the internal calibrator temperature is fully controllable, to allow null measurements. The use of single mode scalar feed horns gives tightly controlled beams with low side lobes. Observing at 90 GHz gives the best combination of low galactic and atmospheric emissivities, and flying at an altitude of 36 km reduces the atmospheric contribution to an almost negligible level of $\simeq$ 1 mK.

To model the atmospheric contribution, we used the JPL line catalog to calculate the antenna temperature as a function of frequency at zenith. This calculation included contributions from water, oxygen and ozone, and assumes a nominal tropospheric water content of 5 g/m^3 (see Figure 6a). These values were then integrated across the bandpasses, and subsequently convolved with the beam, using the theoretical beam shape and the elevation angle used during the measurements, 61° (Figure 6b). The atmospheric antenna temperature is assumed to increase as the secant of the angle from zenith. The result of this calculation is an estimated contribution of 0.92 mK at 98.8 GHz and 1.12 mK at 90 GHz. Previous experience suggests that these calculations are only accurate to approximately a factor of 2, and so to be conservative, an error bar equal to the total expected contribution is chosen.

At 90 GHz and above, the major contribution to the sky temperature from the galax

is expected to come from dust emission. Using our Advanced Cosmic Microwave Explorer (*ACME*) telescope from the South Pole, the emission from the galactic center was measured to be 5 mK at 90 GHz, and this emission came from a region $\approx 0.5°$ across (Meinhold 1993). This is slightly higher than what might be expected by scaling higher frequency data to 90 GHz. If we model this as a 5 mK bar $0.5°$ across and put it at the center of our beam, the measured antenna temperature would be 1/4 mK. Because the entire instrument rotated while making the measurement, the actual contribution is expected to be far less. Thus any contribution from the galaxy is neglected in this analysis.

To model any possible contamination from the 300 K earth, we used a beam which consisted of the theoretical far field beam pattern, with a minimum response of -80 dB at angles far from the beam center. This response was added to model any possible stray pickup, and is suggested by beam patterns measured with other instruments. Convolving this beam with a 300 K earth (elevation angles ≤ 0) gave a contribution of 0.46 mK. Again, to be conservative, we use an error bar equal to 0.46 mK.

The balloon itself can contribute to the measured antenna temperature in two ways. The balloon can emit thermally, and warm radiation from the ground can reflect off the balloon material into the instrument. To reduce both of these effects, it was decided to use a suspension ladder of length 40 meters, twice the standard length. The balloon material was 0.002 cm thick polyethylene, and did not contain the metal tapes commonly used to increase the balloon's radar cross section. The balloon was modeled as a sphere of radius 42.8 meters. The instrument hung 121 meters from the center of the balloon. For the emissivity calculation, an antenna temperature of 70 mK at normal incidence was used, which was scaled from measurements at 31.4 GHz, assuming a loss tangent independent of frequency. For the reflectivity calculation, the beam is convolved with the reflected power from the balloon, and ray tracing is used to determine the angle of incidence on the

balloon. Reflections from the back and front surface are calculated, but multiple reflections are neglected. Only rays that hit the ground, which is assumed isothermal at 300 K, are considered to give any contribution. The calculated contributions from these two sources are 0.3 ± 0.3 mK for emission, and 4.1 ± 4.1 mK for reflection. The assumption that the balloon is spherical, however, is a poor one. The balloon actually has a pear shape, coming to a point at the bottom. This works to reduce the maximum radius, move the point of maximum radius higher, and reflect those rays that do hit the balloon away form the earth. These effects all work to reduce the contributed antenna temperature. This is corroborated by the zenith scan that we took at the end of the flight (see §6 and Figure 7). These data clearly show that the expected contribution from the balloon at the zenith angle of 29° is much smaller than our model, and we therefore neglect the effects of the reflected portion. Another possible source of error is thermal pickup from the warm instrument aperture, made of 6061 Aluminum. As part of the testing before flight, a reflectometer was attached behind the feed horn, and the offset in reflected power was measured as the chopper mirror was alternately moved to the observe and calibrate positions. In the laboratory, no offset was seen at the -80 dB level, and in the field, the measurement was repeated with a noise level of -70 dB. If we assume that any power from the reflectometer incident on the aperture is reflected back into the instrument at a level of -30 dB (which is 10 dB less than that expected from our laboratory work), this would imply a pickup of -40 dB. The expected room temperature emissivity of 6061 Aluminum (resistivity = $.0138 \mu\Omega - \mathrm{cm}$ (Clark et al. 1970), 45° angle of incidence) is 1×10^{-3} and thus the expected pickup from the warm surfaces is of order 10 μK.

A similar calculation shows that the flat chopper mirror, also made of 6061 Aluminum 0.635 cm thick, operating at 10 K and with an assumed 300 K radiant load driving a thermal gradient, should give rise to an offset of 2.1×10^{-12} K. These small errors are neglected. The remainder of the optics are common to both the sky and the calibrate

positions, and thus they should not contribute to the measured offset.

A related offset can arise from standing waves internal to the instrument. This standing wave can give rise to a power offset of

$$2rI\,\mathrm{sinc}\left(\frac{2\Delta\nu l}{c}\right)\cos\left(2kl\right) \tag{4}$$

where r is the voltage reflection coefficient of the source of the internal reflection, $\Delta\nu$ is the bandwidth of the radiated radiation (not more than the bandwidth of the instrument) and l is the distance from the throat of the scalar feed horn to the source of the reflection. I is the power radiated, and can be thermal, in which case the bandwidth is that of the instrument. It can also be very narrow band, for example if it is local oscillator power leakage. As described above, the latter is the source of the measured standing wave in system "B". To set limits to this effect, we again use the fact that the offset measured using the reflectometer setup is less than -70 dB. The calibrator was measured to have a power offset of -60 dB across the band, and thus any other source of standing wave would have to be at least a factor of 3 smaller. The measured standing wave for system "B" was 34 mK, and for system "A" this value was less than 40 mK. Thus the expected offsets are less than 13 mK and 11 mK for systems "A" and "B", respectively. Because these coherent reflections can either add or subtract from the measured antenna temperature, the expected errors are taken to be 0.0 ± 13 mK for "A" and 0.0 ± 11 mK for "B".

The final class of errors involves offsets that do not have their origin in radiation at the radio frequency of the measurements. These include electrical offsets that change with mirror position, pickup from the CIP transmitter or other L-band sources that is modulated by the mirror position, or other sources. To place limits on these offsets, we use data that were taken while the local oscillator was turned off. For example, data set 2, although used as a measurement of T_{CMB}, can be used to constrain the offset of channel "B", because the local oscillator for "B" was turned off. Analyzing this data in an identical fashion to

data set 1 gives -2.5 ± 8.4 mK. Similarly, a long set of data taken with the local oscillator for channel "A" turned off gives 3.7 ± 10.9 mK. The fact that both of these values are much smaller than their statistical error suggests that those errors are conservative. We use 0.0 ± 10.9 and 0.0 ± 8.4 for the offsets of "A" and "B", respectively.

6. RESULTS

All of theses errors are tabulated in Table 1. Adding the amplitudes of the errors to the measured temperatures and doing a quadrature sum of the error bars yields $T_{CMB} = 2.698 \pm 0.020$ K for data set 1 and $T_{CMB} = 2.761 \pm 0.031$ K for data set 3. The largest of these errors, the statistical errors, the errors arising from coherent reflections, and the offset, could have any sign, and there is no reason the expect the two channels to have the same sign. Therefore we are justified in doing a weighted sum of these two measurements which yields our final result, $T_{CMB} = 2.717 \pm 0.017$ K As mentioned previously, we also did at zenith scan to check our models of contaminants that depended on elevation angle. System "B" showed no evidence of atmospheric contamination, as was expected. System "A", which was tuned to observe the ozone line at 101.75 GHz, showed a measured temperature of 90 mK at zenith angles far from the balloon. A least squares fit to a secant was performed, yielding a sky temperature at zenith of 77 mK, which is approximately twice the calculated value of 37 mK. Part of this excess could come from unknown standing wave or electrical offset contributions, with the balance due to inaccuracies in our model atmosphere. As the zenith angle was reduced below 20°, the balloon became visible. From this data, it is quite clear that the pickup from the balloon is small at 20°, and should be quite negligible at the angle at which we took CMB data, 29°. Figure 7 shows this data, along with our model, which includes the balloon and a 77 mK atmosphere. As discussed in §5, the discrepancy at 20° is attributed to the simplifying

assumption that the balloon is spherical.

7. DISCUSSION

During the flight, the instrument performed close to the level at which it proved capable in the laboratory. Except for a frequency shift in channel "B" during launch, all systems performed well.

The two channels in our instrument gave results that are consistent within the errors, suggesting that we do understand the largest errors in the measurements. Our final result, $T_{CMB} = 2.717 \pm 0.017$ K, is the most sensitive measurement to date at 90 GHz. This result is in excellent agreement with the FIRAS measurement of 2.726 ± 0.010 K, and the COBRA result of 2.736 ± 0.017 K. This excellent agreement is especially encouraging considering the fundamental differences between these instruments. It is also in reasonable agreement with the previous ground-based measurements at 3.3 mm. and the cyanogen measurements. The measurement agrees less well with the work of Johnson and Wilkinson. The largest source of error, the statistical errors, could easily be reduced by the use of a rapid Dicke switch at the front end. This would also allow for a more sensitive measurement of the electrical offset. An isolator would eliminate any potential standing wave, although the availability of a cryogenic isolator with an 85-110 GHz bandpass is questionable. However, it seems clear that the sensitivity of this instrument could be made to approach 1 mK, a higher precision than FIRAS or any other measurement. This being the case, and the fact that there is still no measurement of any distortion of the spectrum of the CMB, would seem to argue for more measurements of this kind.

8. CONCLUSION

We have presented results from a two frequency measurement of the temperature of the cosmic background radiation. The instrument was a dual channel coherent radiometer capable of making measurements in the range of 85-110 GHz. The systematic errors common to previous measurements, such as atmospheric emission, galactic contamination, emission from warm optics, and ground pickup, have all been reduced to a level of $\simeq 1$ mK. The final result was $T_{CMB} = 2.717 \pm 0.017$ K. This is consistent with previous similar measurements.

We wish to thank Paul Richards and Donald Morris for many illuminating conversations. The measurements using system "A" would not have been possible without the excellent tunable Gunn diode oscillators built by John Carlstrom. The support of the National Scientific Balloon Facility was extremely professional. Rudi Stuber, Matt Wilson, and the entire UCSB machine shop deserve special thanks. This work was supported by the National Aeronautics and Space Administration, under grant NAGW-1062.

Table 1. Systematic Errors (mK)

System	Atmosphere	Ground	Balloon	Reflections	Offset
"A"	$+0.92 \pm 0.92$	$+0.46 \pm 0.46$	$+0.3 \pm 0.3$	0 ± 13	0 ± 8.4
"B"	$+1.12 \pm 1.12$	$+0.46 \pm 0.46$	$+0.3 \pm 0.3$	0 ± 11	0 ± 10.9

REFERENCES

Alpher, R. A., and Herman, R. C. 1950, Rev. Mod. Phys., 22, 153

Bensadoun et al., 1993, ApJ, 409, 1

Bersanelli, M., Witebsky, C., Bensadoun, M., De Amici, G., Kogut, A., Levin, S., and Smoot, G. F. 1989, ApJ, 339, 632

Clark, A., Childs, G., and Wallace, G. 1970, Cryogenics, 10, 295

Crane, P., Hegyi, D., Kutner, M., and Mandolesi, N. 1989, ApJ, 346, 136

Gamow, G. 1946, Phys. Rev., 70, 572

Gush, H., Halpern, M, and Wishnow, E. 1990 Phys. Rev. Lett., 65, 537

Johnson, D. and Wilkinson, D. 1987, ApJ, 313, L1

Kogut, A., Petuchowski, S., Bennett, C. and Smoot, G. 1990, ApJ, 348, L45

Mather, J. et al., 1994, ApJ, 420, 439

Meinhold, 1993, private communication

Meyer, D. and Jura, M. 1985, ApJ, 297, 119

Negroponte, J. Rowan-Robinson, M., and Silk, J. 1981 ApJ, 248, 38

Penzias, A. and Wilson, R. ApJ., 1965, 142, 414

Ponce, G. A. and Vishniac, E. T. 1988, ApJ, 332, 57

Rees, M. 1968, ApJ, 153, L1

Sanchez, N. and Signore, M. 1990, Phys. Lett. B. 241,13

Schuster, J. and Lubin, P. 1994, Rev. of Sci. Inst., submitted

Sironi, G. et al., 1990, ApJ, 357, 301

Smoot, G. et al. 1987, ApJ, 317, L45

Sunyaev, R. A. and Zel'dovich, Ya. B. 1969, Ap&SS, 4, 301

Sunyaev, R. A. and Zel'dovich, Ya. B. 1970, Ap&SS, 7, 20

Wright, E, et al, 1993 ApJ, 420, 450

This manuscript was prepared with the AAS LaTeX macros v4.0.

Fig. 1.— System layout. For clarity, the off-axis ellipsoidal mirrors have been schematically represented by lenses.

Fig. 2.— Receiver schematic. Includes RF and IF components.

Fig. 3.— Balloon Gondola.

Fig. 4.— Calibrator Temperature and system "B" output during small signal calibrations.

Fig. 5.— Data set 1. (a) Shows the measured standing wave as a function of calibrator position and the best fit standing wave, while (b) shows the residuals of the fit to this standing wave.

Fig. 6.— Expected antenna temperature at 36 km altitude and 29 ° from zenith. (a) shows the atmospheric power spectrum, and (b) shows this spectrum convolved with the beam and integrated across the instrument band pass.

Fig. 7.— Data from zenith scan with model. Model includes balloon emission, reflection of 300 K radiation from the ground, and 77 K atmosphere.

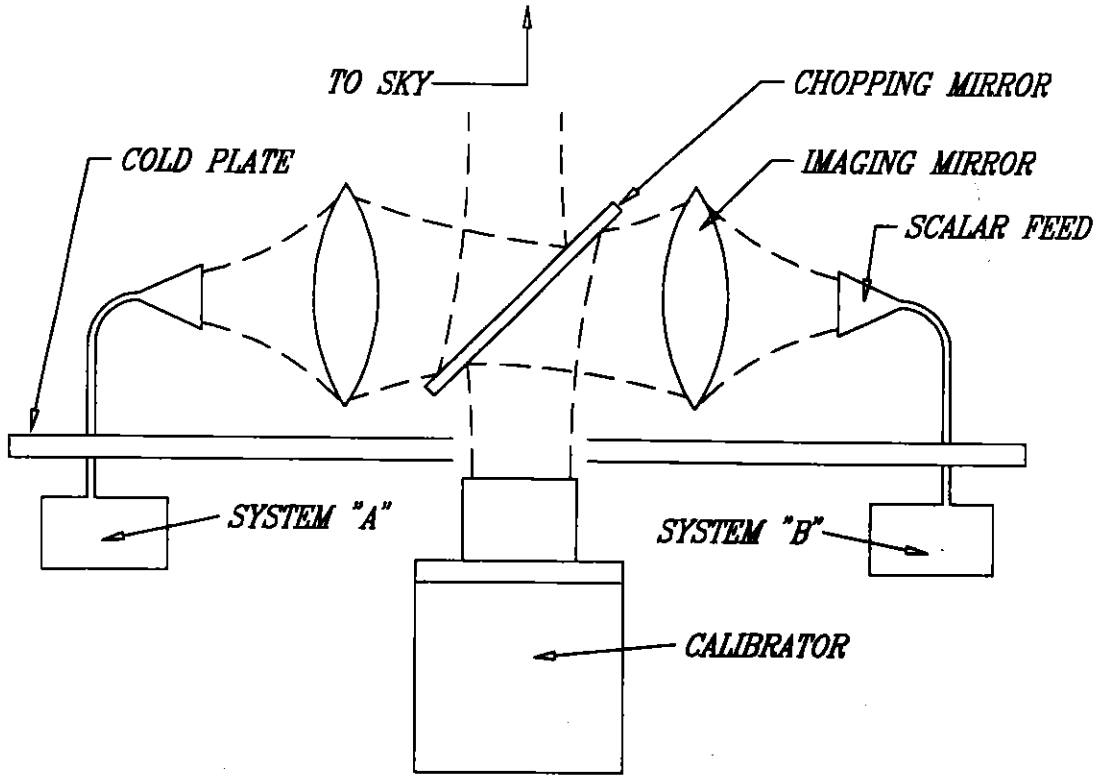
TO SKY
CHOPPING MIRROR
COLD PLATE
IMAGING MIRROR
SCALAR FEED
SYSTEM "A"
SYSTEM "B"
CALIBRATOR

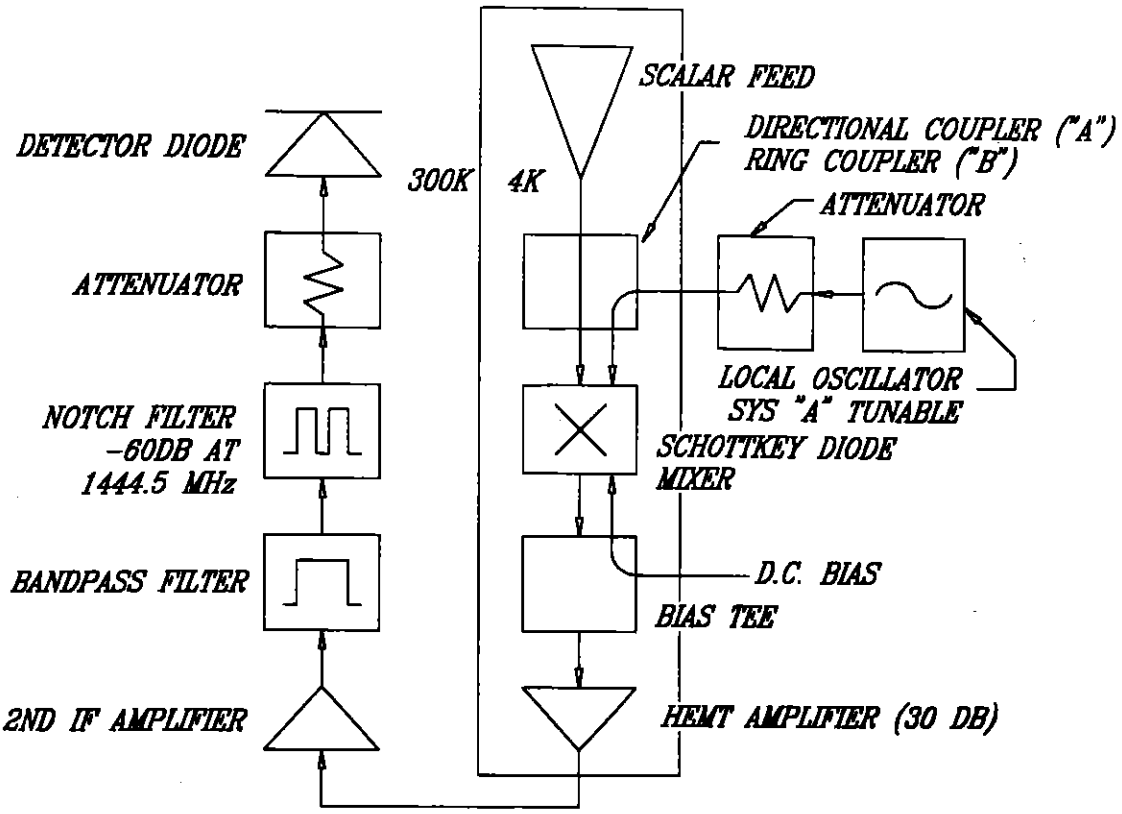
SCALAR FEED
DETECTOR DIODE
DIRECTIONAL COUPLER ("A")
RING COUPLER ("B")
300K
4K
ATTENUATOR
ATTENUATOR
LOCAL OSCILLATOR
SYS "A" TUNABLE
NOTCH FILTER
-60DB AT
1444.5 MHz
SCHOTTKEY DIODE
MIXER
D.C. BIAS
BANDPASS FILTER
BIAS TEE
2ND IF AMPLIFIER
HEMT AMPLIFIER (30 DB)

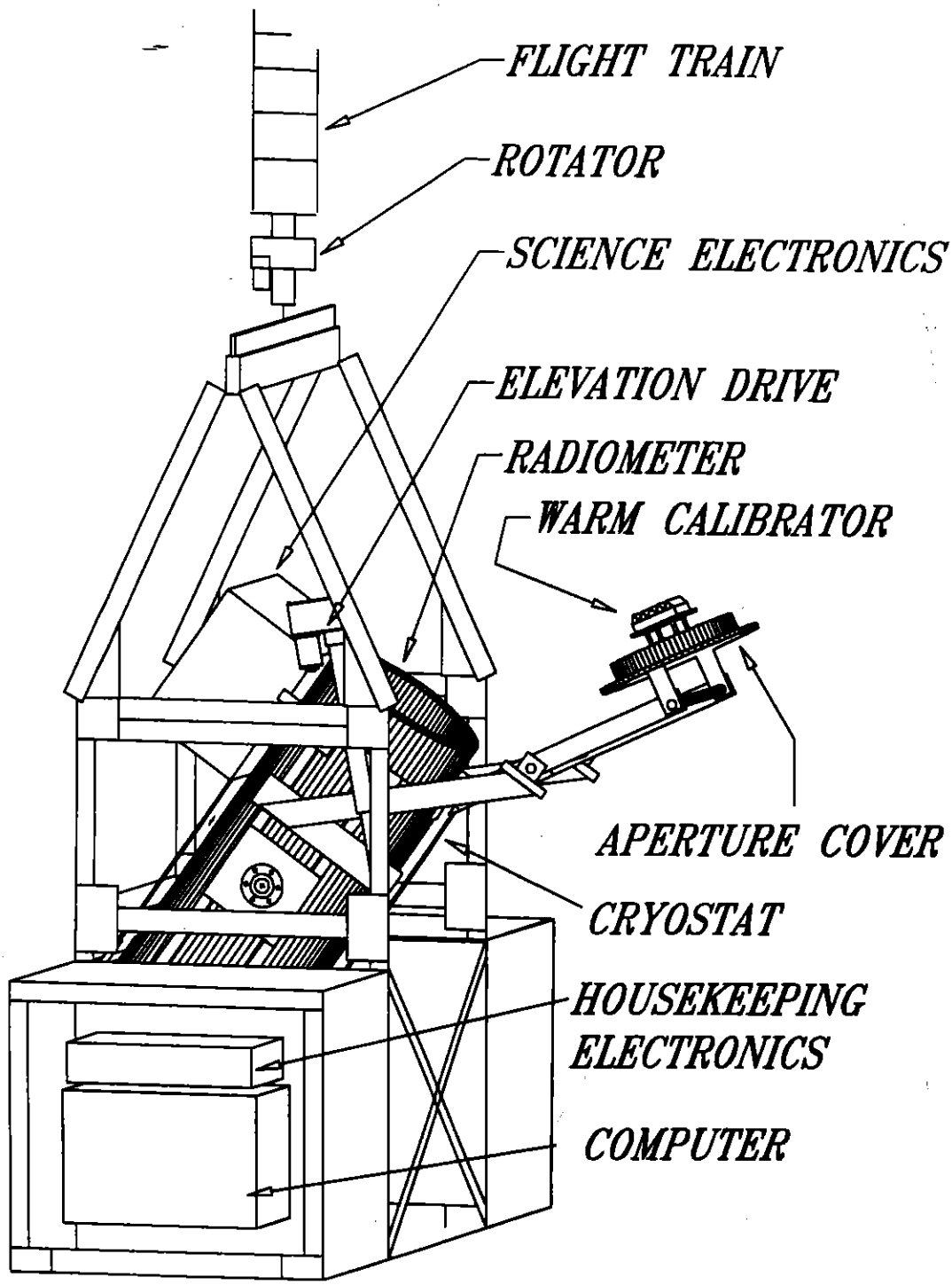
FLIGHT TRAIN
ROTATOR
SCIENCE ELECTRONICS
ELEVATION DRIVE
RADIOMETER
WARM CALIBRATOR
APERTURE COVER
CRYOSTAT
HOUSEKEEPING ELECTRONICS
COMPUTER

Fig 3

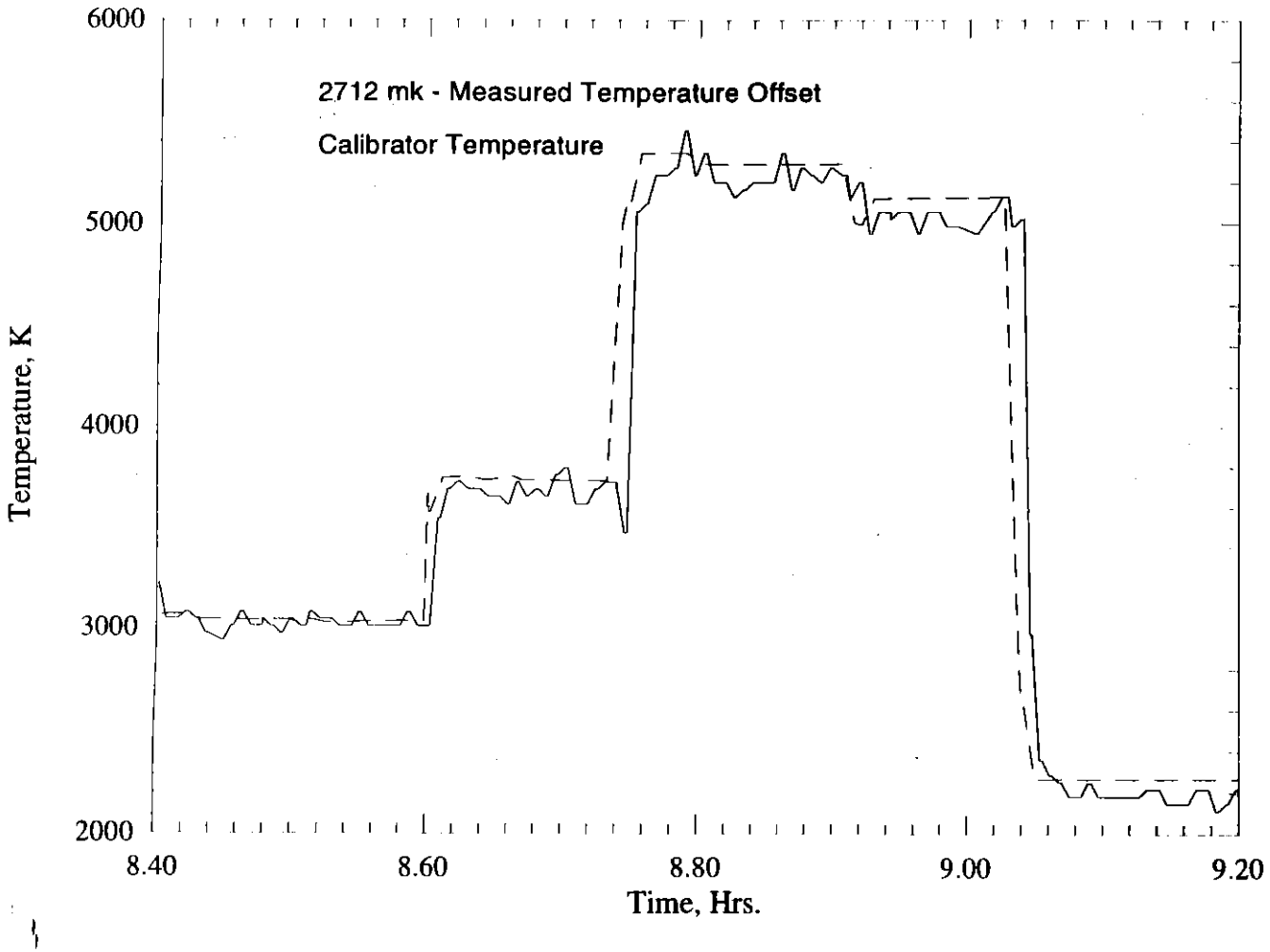
2712 mk - Measured Temperature Offset
Calibrator Temperature
Temperature, K
6000
5000
4000
3000
2000
8.40
8.60
8.80
9.00
9.20
Time, Hrs.

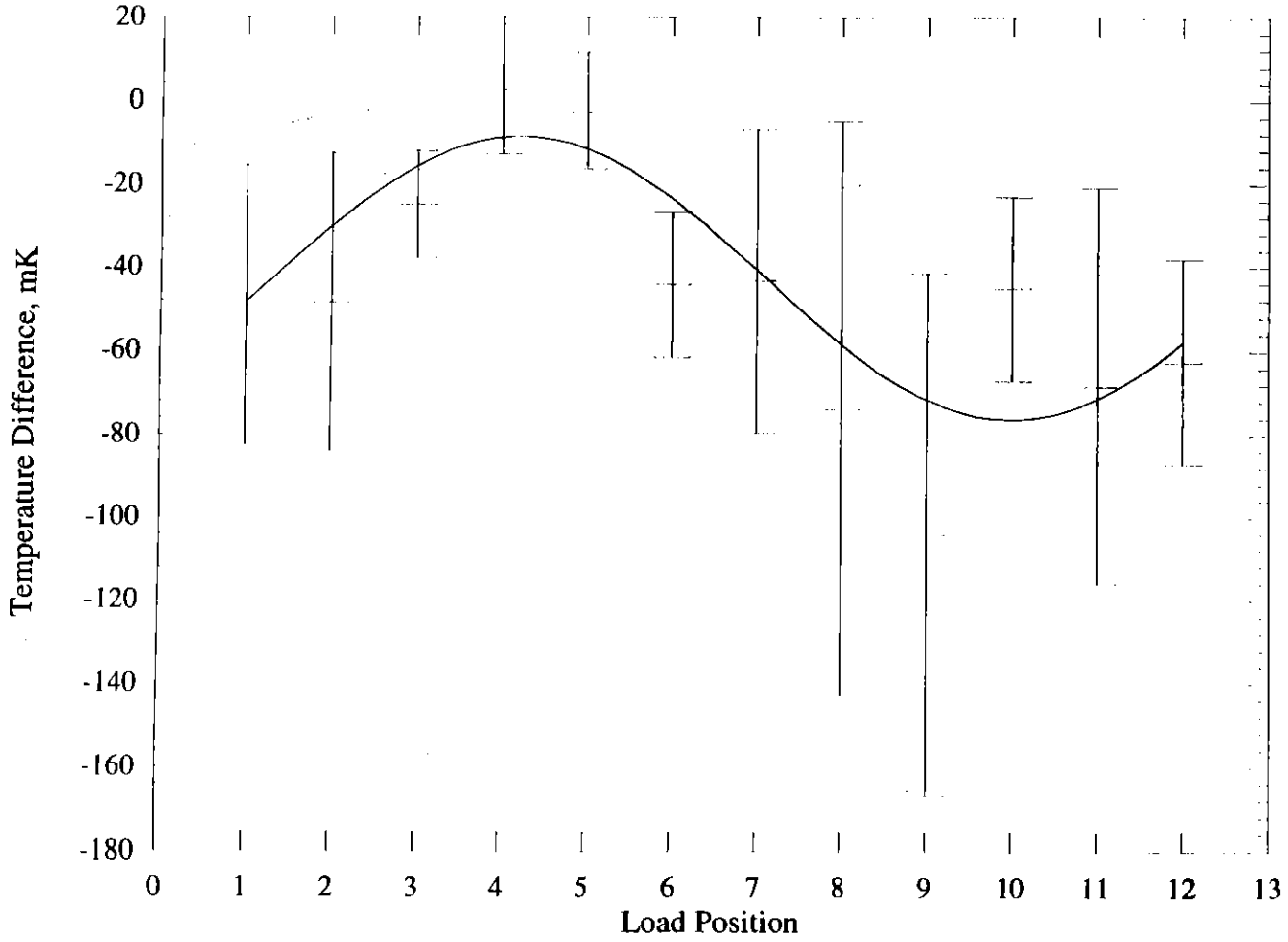
20
0
-20
-40
-60
-80
-100
-120
-140
-160
-180
Temperature Difference, mK
0
1
2
3
4
5
6
7
8
9
10
11
12
13
Load Position

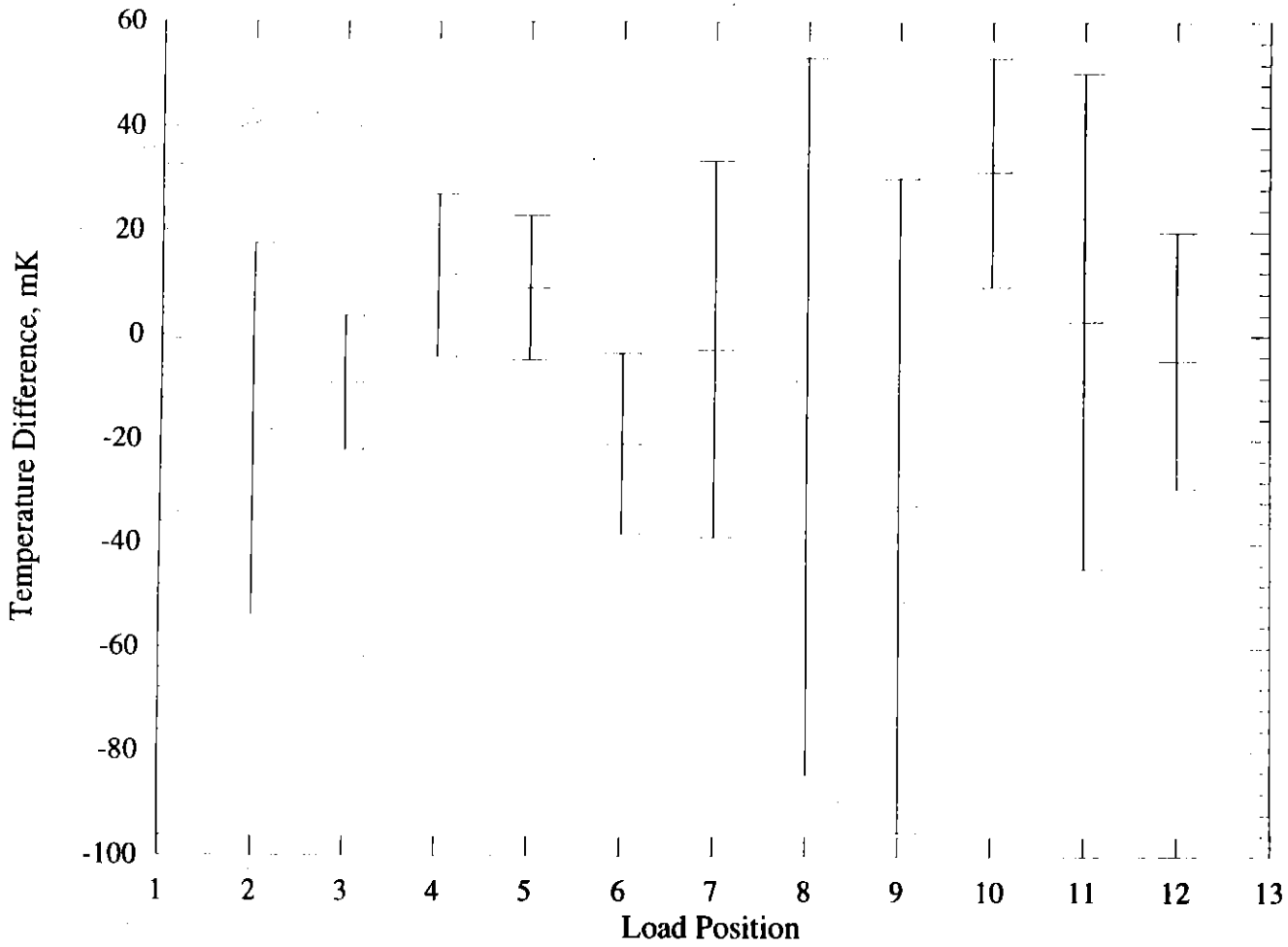
60
40
20
0
-20
-40
-60
-80
-100
Temperature Difference, mK
1
2
3
4
5
6
7
8
9
10
11
12
13
Load Position

Fig 5

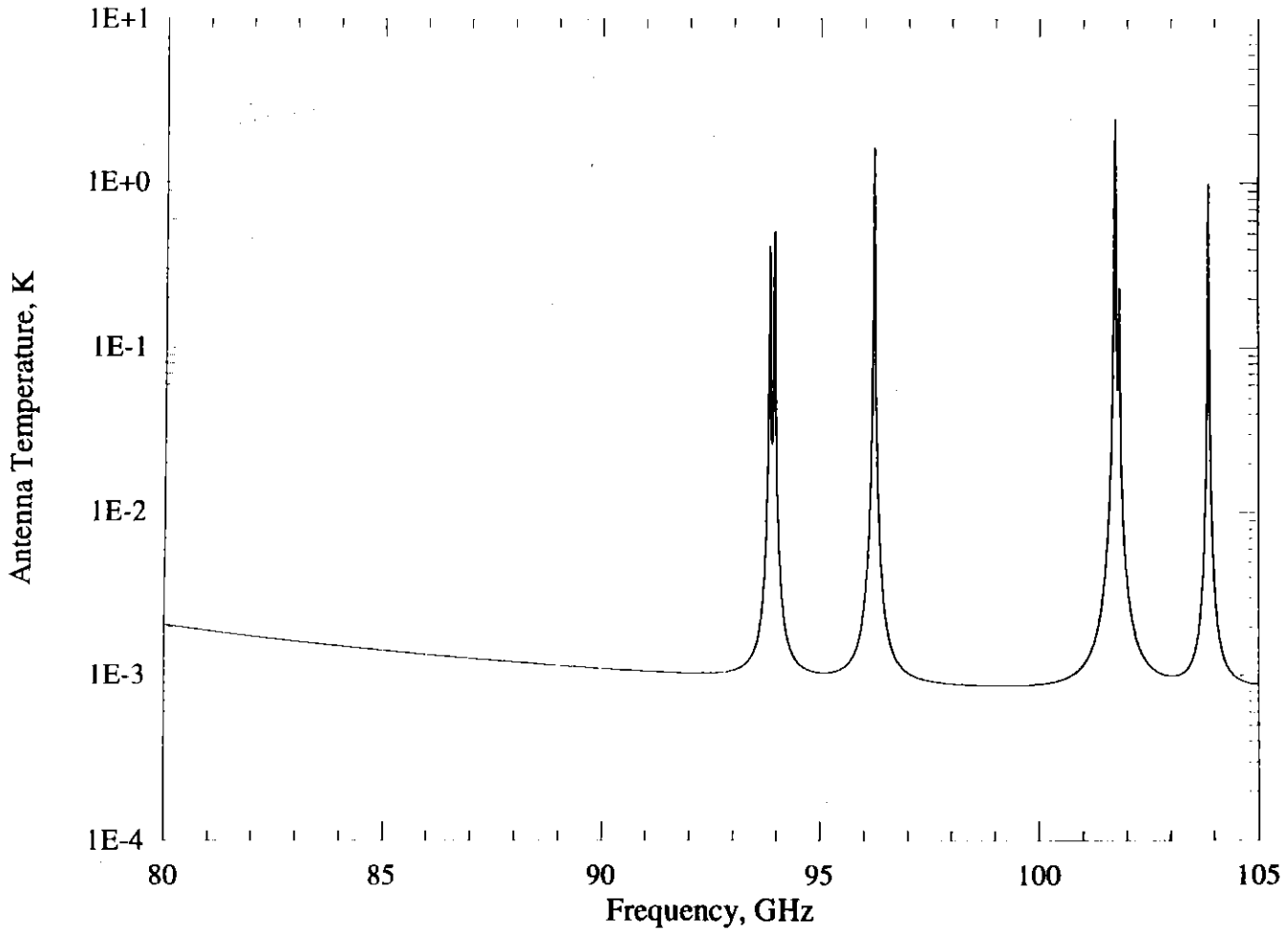
1E+1
1E+0
1E-1
1E-2
1E-3
1E-4
Antenna Temperature, K
80
85
90
95
100
105
Frequency, GHz

Fig 6a

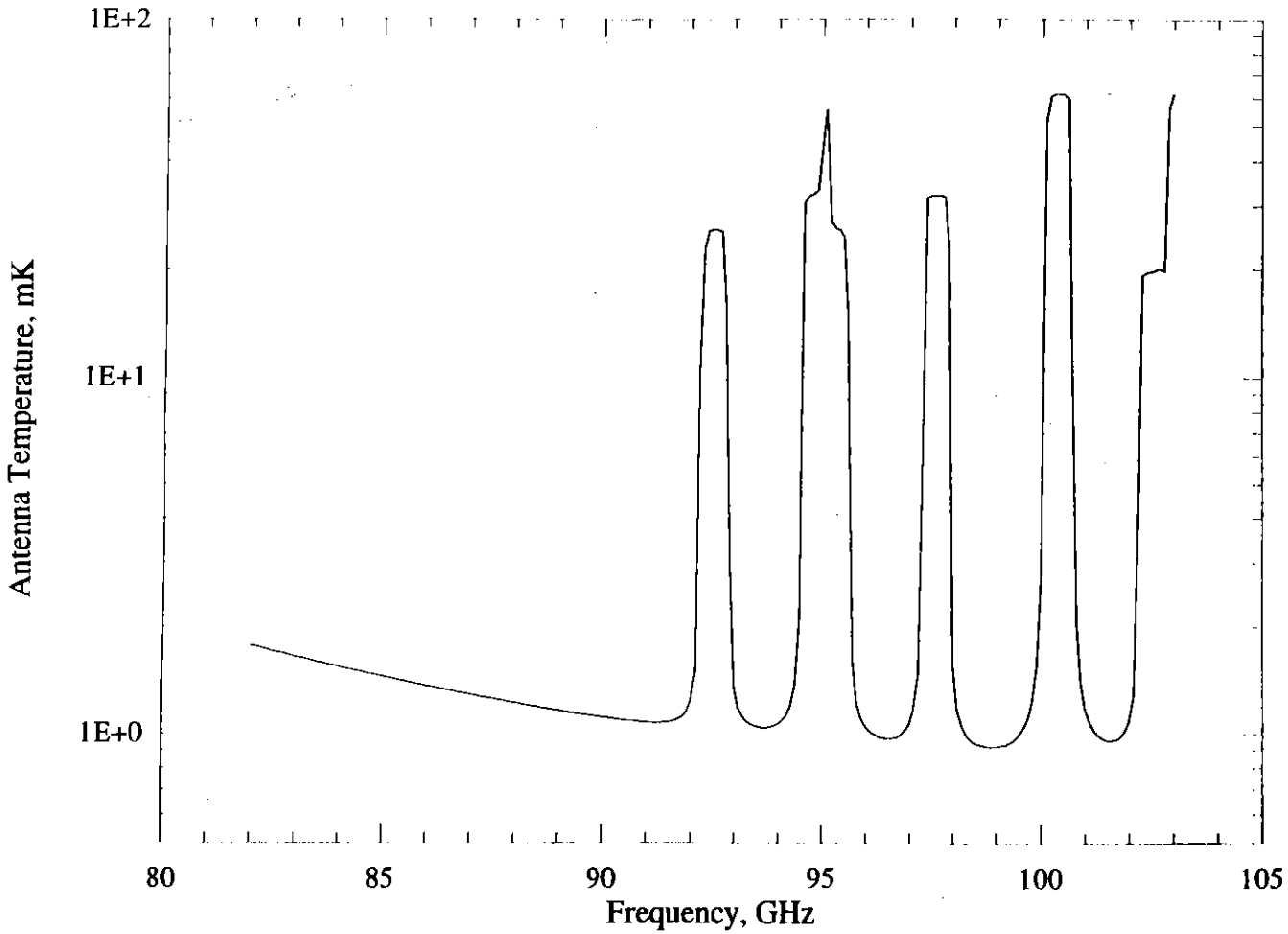
1E+2
1E+1
1E+0
Antenna Temperature, mK
80
85
90
95
100
105
Frequency, GHz

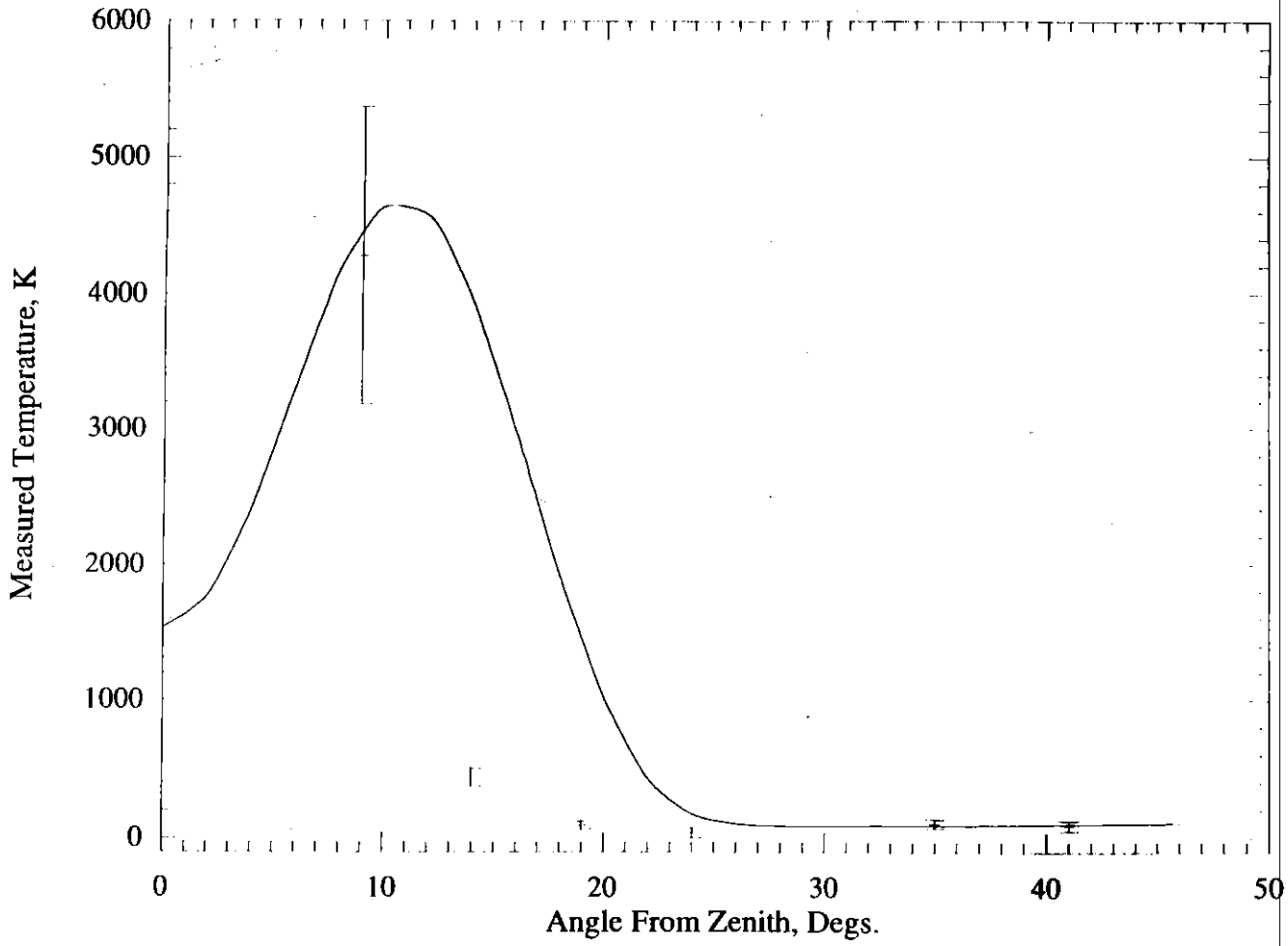
6000
5000
4000
3000
2000
1000
0
Measured Temperature, K
0
10
20
30
40
50
Angle From Zenith, Degs.

Fig 7